

# Improved Belief Propagation Decoding on Surface Codes with High Accuracy and Low Latency

Jiahan Chen, Zhipeng Liang, Zhengzhong Yi, and Xuan Wang

Harbin Institute of Technology, Shenzhen, China

Quantum error correction is crucial for universal quantum computing, requiring highly accurate and low-latency decoding algorithms. Belief Propagation (BP) is notable for its linear time complexity and general applicability to quantum LDPC codes. However, BP performs poorly on highly degenerate codes without Order Statistic Decoding (OSD) post-processing, which significantly increases time complexity. We focus on improving BP's performance on surface codes. We first propose Momentum-BP and AdaGrad-BP, inspired by machine learning optimization techniques, to reduce the oscillation of message updating and break the symmetric trapping sets. We further propose EWAInit-BP, which adaptively updates initial probabilities and exhibits aggressive exploration capabilities. EWAInit-BP achieves the highest accuracy among BP improvements without OSD post-processing on planar surface code, toric code, and XZZX surface code, providing a 1~3 orders of magnitude improvement compared to traditional BP, and demonstrating the error correction capability even under parallel scheduling. Its theoretical  $O(1)$  time complexity and high accuracy make it a promising candidate for high-precision real-time decoders.

## 1 Introduction

Information in quantum computing devices is highly susceptible to noises and interference, leading to information loss and computational errors [1]. To address this issue, quantum error correction (QEC) technology introduces redundant qubits and uses quantum error-correcting codes

Zhengzhong Yi: [zhengzhongyi@stu.hit.edu.cn](mailto:zhengzhongyi@stu.hit.edu.cn)

to protect the integrity of quantum information. In fact, QEC is an essential step towards achieving fault-tolerant quantum computation [2].

Most existing quantum error correction codes are based on stabilizer framework [3]. Surface codes are a special class of stabilizer codes where qubits are placed on a 2D lattice [4]. These codes, especially the planar surface code have received significant attention over the past two decades [5–7] due to the local connections between stabilizers and qubits and high circuit-level threshold [8]. The planar surface code is defined on the lattice with open boundaries, which can reduce engineering requirements [9]. The toric code, on the other hand, is encoded in a torus-like structure with periodic boundaries, featuring complete boundary stabilizers and thus slightly stronger error-correcting capabilities [10]. The XZZX surface code is an improvement over the planar surface code, offering strong performance under biased noise [11]. All the three codes have the code distance scaling with the code length as  $O(\sqrt{N})$  but have asymptotically vanishing code rates.

There are several decoding algorithms suitable for surface codes. The Minimum-Weight Perfect Matching (MWPM) algorithm [12] achieves a code capacity threshold of approximately 15.5% for the planar surface code under depolarizing noise, but its time complexity is  $O(N^3)$ . The Tensor Network Contraction method [13] achieves a very high threshold of 18.3%, but its time complexity is  $O(N\gamma^3)$ , where  $\gamma$  controls the approximation accuracy. The Renormalization Group method [14] achieves a threshold of 15.2%, with the time complexity of  $O(N \log \sqrt{N})$ . The Union-Find method [15] has near-linear complexity  $O(N\alpha)$ , but it achieves a slightly lower threshold of 14.8%. However, the aforementioned methods can hardly simultaneously meet the requirements for high accuracy and low latency in quantum error correction decoding [16, 17].

Belief Propagation (BP) algorithm [18] are ap-

plicable to any sparse quantum code and can achieve a linear complexity of  $O(j\tau N)$ , where  $j$  is the average weight of the rows/columns of the check matrix, and  $\tau$  is the number of iterations. Additionally, parallel scheduling of BP can be efficiently implemented in hardware, theoretically achieving constant-time complexity [19]. However, traditional BP exhibit low accuracy for many quantum error correcting codes and even cannot achieve the code capacity threshold for surface codes. BP can be implemented in both quaternary [20–26] and binary domain [27–30]. There have been some improvements that enable BP to demonstrate error-correcting capabilities on surface codes (i.e., logical error rates decrease as code length increases). In the quaternary domain, MBP [25] achieves a threshold of 14.5%~16% on the planar surface code by modifying the step size in the *a posteriori* probability updating. However, MBP can only implemented in serial scheduling, and the outer loop for searching step sizes increases its time complexity. In the binary domain, GBP [30] achieves a 14% threshold by combining generalized belief propagation with multiple rounds of decoding. This algorithm can be implemented in parallel, but the number of outer loops increases with the code length, adding to its time complexity. BP-OTS [31] periodically detects and breaks trapping sets using manually set parameters, allowing parallel implementation while maintaining the original complexity. It outperforms MBP for short codes but does not achieve a significant threshold.

BP can also be combined with post-processing methods, such as BP-MWPM [32–34], BP-SI (stabilizer inactivation) [35]. Although these algorithms can achieve high thresholds for surface codes, they all have high time complexities, ranging from  $O(N^2)$  to  $O(N^3)$ . For example, BP-OSD [36–38] is renowned for its high thresholds on most sparse quantum codes, particularly achieving 17.68% on planar surface codes [39]. However, even using the lowest 0-order OSD, the time overhead in hardware is unacceptable for real-time decoding [19]. Enhancing BP performance without relying on post-processing algorithms remains a significant challenge.

There are several explanations for why surface codes are challenging for BP decoding. From the perspective of degeneracy [25, 40], stabilizers of surface codes have much lower weights com-

pared to the code distance, leading to multiple low-weight errors corresponding to the same syndrome, thus complicating BP’s error convergence. From the perspective of short cycles [18], a number of 4-cycles in the quaternary domain and 8-cycles in the binary domain in surface codes can cause BP’s inaccurate updating. A more intuitive explanation involves trapping sets [31, 41], where surface codes have many symmetric trapping sets causing BP messages to oscillate periodically.

This paper employs three strategies for improving BP: optimizing message updates, optimizing prior probabilities, and utilizing iterative feedback information. First, we leverage the similarity between BP posterior updating and gradient descent of the energy function, drawing inspiration from optimization methods in machine learning to enhance the message update rules. In addition to reducing the logical error rate of decoding, experiments on trapping sets in surface codes show that our proposed method, Momentum-BP and AdaGrad-BP, can smooth the message update direction and reduce oscillation amplitude.

Furthermore, recognizing the importance of prior probabilities from the probabilistic derivation of BP, we extend the idea of optimizing message updates to an adaptive approach, EWAInit-BP, to dynamically update the *a priori* probabilities involved in each iteration. Experiments on short toric codes, planar surface codes, and XZZX surface codes (under bias noise) show that EWAInit-BP outperforms existing BP improvements without post-processing while demonstrating error correction capabilities on both parallel scheduling and serial scheduling. Notably, the time complexity of all proposed improvements remains  $O(j\tau n)$ . Thus, EWAInit-BP can be implemented with theoretical constant complexity in parallel while maintaining decoding accuracy.

The structure of this paper is as follows. Section 2 introduces the fundamentals of surface codes and BP decoding, as well as the perspective of BP as a gradient optimization, and summarizes the challenges BP faces in decoding surface codes. Section 3 first optimizes BP’s message update rules, and then applies these ideas to the adaptive initialization. The results of the simulation are presented in Chapter 4. Finally, Chapter 5 summarizes our work and discusses the existing challenges.

## 2 Preliminaries

### 2.1 Surface codes

A stabilizer code is defined by an abelian subgroup  $\mathcal{S}$  of the Pauli group  $\mathcal{P}_n$  excluding  $-I$ , composed of operators  $S \in \mathcal{P}_n$  such that  $S|\psi\rangle = |\psi\rangle$  for all codewords  $|\psi\rangle$  in the code space. The code space is the simultaneous  $+1$  eigenspace of all elements of  $\mathcal{S}$ . The stabilizers must commute with each other, which means  $[S_i, S_j] = 0$  for all  $S_i, S_j \in \mathcal{S}$ . The dimension of the code space is determined by the number of independent generators of  $\mathcal{S}$ . For a stabilizer code with  $N$  physical qubits and  $K$  logical qubits,  $\mathcal{S}$  has  $N - K$  independent generators.

The stabilizers are used to detect errors by measuring their eigenvalues. The set of measurement outcomes, known as the *error syndrome*, indicates the presence and possibly the location of errors. Logical operators are Pauli operators that commute with all elements of  $\mathcal{S}$  but are not themselves in  $\mathcal{S}$ , thus in  $\mathcal{N}(\mathcal{S}) \setminus \mathcal{S}$  where  $\mathcal{N}(\mathcal{S}) = \{E : ES = SE, \forall S \in \mathcal{S}\}$ . They act on the encoded logical qubits without disturbing the code space, thus cause an *undetectable error*. The code distance  $D$  is defined as the minimum weight of logical operators. Therefore, a quantum stabilizer code can be represented by  $[[N, K, D]]$ .

Surface codes are a class of quantum Low-Density Parity-Check (LDPC) codes [42] where qubits are placed on a 2-dimensional lattice, relying on the topology of the surface to protect quantum information [4]. Logical qubits are encoded in global degrees of freedom, and larger lattices provide larger code distances. There are some common properties between different types of surface codes, such as the code distance scales with the code length as  $O(\sqrt{N})$ , while the code rate is asymptotically zero.

The  $[[2L^2, 2, L]]$  toric code has a 2-dimensional torus topology, and the closed boundary makes it translationally invariant to the error syndrome, which is beneficial to decoding algorithms (such as BP and neural networks). The Euler characteristic of the torus is 0, but the X and Z stabilizers of the toric code each have a redundancy, resulting in a total of two encoded logical qubits.

The  $[[2L^2 - 2L + 1, 1, L]]$  planar surface code is defined on a surface with open boundaries, which makes the stabilizers near the boundaries having lower weights. This reduction in stabilizer weight

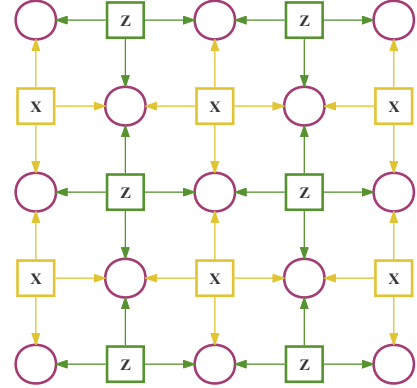


Figure 1: The lattice of the  $[[2L^2 - 2L + 1, 1, L]]$  planar surface code for  $L=3$ . Circles represent data qubits, yellow squares represent X-type stabilizers, green squares represent Z-type stabilizers, and arrows indicate the coupling between stabilizers and qubits.

results in a slight decrease in the error correction capability compared to the toric code, however, simplifies its implementation in physical quantum systems. The lattice structure of the planar surface codes are illustrated in Fig. 1.

The  $[[L^2, 2, L]]$  XZZX surface code is a non-CSS code designed to handle biased noise more effectively. The stabilizers of the family of code have the form of XZZX. This alternating pattern of Pauli-X and Pauli-Z operators allows the code to reach the theoretical maximum threshold of 50% for certain types of noise.

### 2.2 Belief propagation decoding

#### 2.2.1 BP in the quaternary logarithmic domain

The idea of *maximum likelihood decoding* in quantum error correction is to find the most likely error coset given the error syndrome. This can be expressed as [20]

$$E = \arg \max_{ES} \sum_{S \in \mathcal{S}} p(ES|s) \quad (1)$$

where the term  $ES$  denotes the coset formed by the error  $E$  and the stabilizer  $S$ . However, finding this maximum likelihood solution is computationally exponential [43]. Belief propagation decoding algorithm simplifies the above objective to

$$E = \left\{ \arg \max_{E_j} p(E_j|s) \right\}_{j=1}^n \quad (2)$$

where the probability of each individual error  $E_j$  given the syndrome  $s$  is maximized independently for  $j = 1$  to  $n$ . Belief propagation makes

two simplifications to the objective, compromising its performance on highly degenerate quantum codes.

- Assuming the most likely error pattern is the same as the most likely error coset;
- Assuming the most likely error on each qubit is the same as the most likely error pattern.

BP algorithm passes messages on a *Tanner graph*, where stabilizers and qubits are represented as *check nodes* and *variable nodes*, respectively. In the quaternary representation which this paper mainly focuses on, each variable node corresponds to a probability vector of all Pauli errors on one qubit.

The quaternary logarithmic domain belief propagation (abbreviated as LLR-BP<sub>4</sub>) receives *a priori* probability vectors describing each type of Pauli error on each qubit  $Q^{(0)} = \{p_{v_j}^X, p_{v_j}^Y, p_{v_j}^Z\}_{j=1}^N$ , and initializes the variable-to-check messages as [25]

$$m_{v_j \rightarrow c_i}^{(0)} = \lambda_{H_{ij}}(Q_{v_j, e}^{(0)}) = \lambda_{H_{ij}}(\ln \frac{1 - p_{v_j}}{p_{v_j}}), \quad (3)$$

where the lambda function is defined as

$$\lambda(p^X, p^Y, p^Z) = \ln \frac{1 + e^{-p^{H_{ij}}}}{e^{-p^X} + e^{-p^Y} + e^{-p^Z} - e^{-p^{H_{ij}}}} \quad (4)$$

indicating the log-likelihood ratio of whether the Pauli error  $E_j$  commutes with the stabilizer  $S_i$ .

In the horizontal updates, each check node calculates the feedback based on the messages received from the variable nodes but not relying on the target variable node, sending a check-to-variable message

$$w = 2 \tanh^{-1} \left( \prod_{v_{j'} \in \mathcal{N}(c_i) \setminus v_j} \tanh \left( \frac{m_{v_{j'} \rightarrow c_i}^{(t-1)}}{2} \right) \right), \quad (5)$$

$$m_{c_i \rightarrow v_j}^{(t)} = (-1)^{s_i} * w. \quad (6)$$

In the vertical updates, variable nodes aggregate the messages from check nodes and, after a similar extrinsic calculation, send variable-to-check messages

$$m_{v_j \rightarrow c_i}^{(t)} = \lambda_{H_{ij}}(Q_{v_j, e}^{(0)} + \sum_{\substack{c_{i'} \in \mathcal{M}(v_j) \setminus c_i \\ \langle e, H_{ij} \rangle = 1}} m_{c_{i'} \rightarrow v_j}^{(t)}). \quad (7)$$

In the hard decision, variable nodes first accumulate the messages from all check nodes to calculate the *a posteriori* probability

$$Q_{v_j, e}^{(t)} = Q_{v_j, e}^{(0)} + \sum_{\substack{c_i \in \mathcal{M}(v_j) \\ \langle e, H_{ij} \rangle = 1}} m_{c_i \rightarrow v_j}^{(t)}. \quad (8)$$

Then, for each variable node, if all log-likelihood ratios (LLR) for Pauli errors are greater than 0, then the hard decision result is I; otherwise, it is the Pauli error with the smallest LLR value. The hard decisions of all qubits combine to form the error estimate  $\hat{E}$ . If  $\hat{E}$  corrects the error syndrome, the algorithm converges; otherwise, it returns to the horizontal update for a new iteration. If the maximum number of iterations is reached, decoding is considered to have failed.

BP can be performed using either parallel or serial scheduling [44]. In parallel scheduling, all variable nodes and check nodes update their messages simultaneously at each iteration, allowing for hardware parallelization, potentially achieving constant complexity. On the other hand, the serial scheduling updates the messages of variable nodes and check nodes sequentially. This method leads to faster convergence and slightly higher accuracy, though it has a more complex hardware implementation.

### 2.2.2 BP as gradient optimization

Each iteration of BP can be interpreted as one step of gradient descent with a simplified step size on the following energy function [25, 45]

$$J_S(\Gamma) = - \sum_{i=1}^m 2 \tanh^{-1} \left( (-1)^{s_i} \prod_{v_j \in \mathcal{N}(c_i)} \tanh \left( \frac{\lambda_{H_{ij}}(Q_{v_j})}{2} \right) \right). \quad (9)$$

The term inside the parentheses of the energy function  $J_S$  measures the discrepancy between the result of the current iteration and the actual error syndrome of stabilizer  $S_i$ . The smaller the energy function, the closer the BP iteration result is to the correct solution.

The target variables for gradient updates are the *a posteriori* estimates of the probability of each type of Pauli error occurring at each variable node. Specifically, for the  $e \in \{X, Y, Z\}$

type Pauli error on the  $n$ -th variable node, the *a posteriori* probability update is

$$Q_{v_j,e}^{(t)} = Q_{v_j,e}^{(t-1)} - \alpha \frac{\partial J}{\partial Q_{v_j,e}^{(t-1)}}, \quad (10)$$

where the partial derivative is

$$\begin{aligned} \frac{\partial J}{\partial Q_{v_j}^e} = & - \sum_{\substack{c_i \in \mathcal{M}(v_j) \\ \langle e, H_{ij} \rangle = 1}} \tilde{m}_{c_i \rightarrow v_j} \\ & * \frac{\eta g_{ij}(\Gamma) e^{-Q_{v_j}^e}}{e^{-Q_{v_j}^X} + e^{-Q_{v_j}^Y} + e^{-Q_{v_j}^Z} - e^{-Q_{v_j}^{H_{ij}}}}, \end{aligned} \quad (11)$$

where  $\tilde{m}_{c_i \rightarrow v_j}$  is the *a posteriori* probability summation term approximated using  $\tanh$

$$\tilde{m}_{c_i \rightarrow v_j} = (-1)^{s_i} \prod_{v_{j'} \in \mathcal{N}(c_i) \setminus v_j} \tanh \left( \frac{\lambda_{H_{ij'}}(\Gamma_{v_{j'}})}{2} \right). \quad (12)$$

From this gradient optimization perspective, MBP [25] adjusts the "learning rate" of message updates to converge more quickly to the equivalent energy minimum, which is common in degenerate quantum codes.

### 2.2.3 Hardness of BP decoding on surface codes

BP without post-processing algorithms perform poorly on surface codes due to factors from multiple perspectives.

**Cycles** Short cycles cause the joint probability calculations in BP to be dependent, which violates the independence assumption of updating variable nodes Eq. (7) and check nodes Eq. (5) [18]. Surface codes exhibit 8-cycles in the binary representation and 4-cycles in the quaternary representation, exacerbating this issue.

**Degeneracy** High degeneracy leads to BP decoding objectives Eq. (2) deviating from true targets Eq. (1) [20, 40]. This problem becomes particularly severe when errors can combine with stabilizers to form error types that are symmetric to original ones. In such cases, BP's marginal probability calculations for the both error types will be completely consistent. In surface codes, weights of the stabilizers are all no greater than 4, often much less than the weights of the logical operators. This symmetric degeneracy results in incorrect convergence of BP decoding.

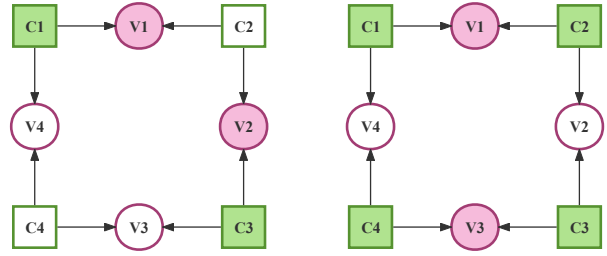


Figure 2: Trapping sets with two types of error patterns in surface codes. Solid circles represent error qubits, and solid squares represent stabilizers with non-trivial error syndromes. The stabilizers in the figure can be either all X-type or all Z-type.

**Trapping Sets** Trapping sets are specific local structures in error-correcting codes combined with corresponding error patterns, where iterative decoding algorithms can never converge [46–48]. In quantum error correction, trapping sets are caused by the aforementioned short loops and symmetric degeneracy [41, 49]. The smallest trapping set in surface codes is shown in Fig. 2, consisting of an 8-cycle and four symmetric stabilizers, where the local connections of each check node and variable node are identical [31]. If any two qubits in this trapping set experience errors that anticommute with the stabilizers, the hard decision result of BP will oscillate periodically between all 0s and all 1s.

Optimizing BP from the first two perspectives involves modifying the underlying principles of the algorithm. This paper will focus on trapping sets and seek methods to break the symmetry in message passing.

## 3 Belief Propagation Optimization

Surface codes violate the assumptions of BP's objective function and probability independence, making BP decoding difficult to converge. These issues are manifested in symmetric trapping sets, where the local structure of each node is identical, and message updates are symmetric under specific error patterns. Breaking the former symmetry involves modifying the code structure, while in this section, we focus on breaking the latter, the symmetry of message updates. Notably, the algorithms proposed in this chapter preserve the same time complexity as traditional belief propagation.

### 3.1 Message updates optimization

#### 3.1.1 Update direction smoothing

The Exponential Weighted Average (EWA) updates and smooths data series by combining the current observation with a weighted average of the previous value, expressed as

$$v_t = \gamma v_{t-1} + (1 - \gamma)x_t, \quad (13)$$

where  $x_t$  is the observation at time  $t$ ,  $v_t$  is the smoothed value, and  $\gamma$  is a decay factor.

In the field of machine learning, momentum methods utilize an idea similar to EWA, adding a momentum term to allow gradient descent to accumulate historical information

$$m_t = \gamma m_{t-1} + (1 - \gamma)\nabla J(\theta), \quad (14)$$

$$\theta = \theta - \alpha m_t, \quad (15)$$

where  $\gamma$  is the decay factor,  $m_t$  is the accumulated momentum term,  $\nabla J(\theta)$  is the gradient of the loss function with respect to parameter  $\theta$ , and  $\alpha$  is the learning rate. This method integrates previous directions while updating each parameter, thereby smoothing the update direction.

BP decoding can be analyzed from the perspective of the energy function. The high degeneracy of surface codes causes the energy function to have many equivalent global minima within a neighborhood. In the case of symmetric trapping sets, BP's specific update step size causes the hard decision results to oscillate between adjacent erroneous solutions. We incorporate the concept of momentum into BP's *a posteriori* probability updates to solve this issue by breaking the symmetry in BP's message updates.

Momentum-BP can be implemented in both parallel and serial scheduling. Here, we provide the latter in algorithm 1, where the initialization and check node update remain the same as in traditional BP. Our approach computes the *a posteriori* probability before performs the vertical update. The posterior update rule of Momentum-BP is shown as Eq. (16) and Eq. (17) where  $g_{v_j,e}^{(t)}$  are the accumulated momentum term and  $Q_{v_j,e}^{(t)}$  are the *a posteriori* probability for the  $j$ -th variable node regarding the Pauli error  $e$  in the  $t$ -th iteration. Notice that we transformed Eq. (8), so that the accumulated term is the posterior

value from the previous iteration. In the variable node update step, we subtract the original message sent from the check node rather than the momentum-smoothed message to ensure stability and prevent overcompensation.

**Algorithm1** Momentum-BP under Serial Scheduling for Quaternary Log Domain

**Input:** Quaternary parity-check matrix  $\mathbf{H}$  of  $M \times N$ , syndrome vector  $\mathbf{s} = (1, -1)^M$ , *a priori* probability vectors  $\{p_{v_j}^X, p_{v_j}^Y, p_{v_j}^Z\}_{j=1}^N$ , max iterations  $iter_{max}$ , learning rate  $\alpha = 1$ , and momentum rate  $\gamma \geq 0$ .

**Output:** Estimated error vector  $\hat{\mathbf{E}}$ .

**Initialization:**

**for**  $j = 1 \rightarrow N$ ,  $e \in \{X, Y, Z\}$ , **do**

    Initialize  $Q_{v_j,e}^{(0)}$  as Eq. (3)

**Serial update:**

**for**  $j = 1 \rightarrow N$ ,  $e \in \{X, Y, Z\}$ , **do**

**for**  $i \in \mathcal{N}(v_j)$ , **do**

        Calculate  $m_{c_i \rightarrow v_j}^{(t)}$  as Eq. (5)

**Momentum update**

$$g_{v_j,e}^{(t)} = \gamma g_{v_j,e}^{(t-1)} + (1 - \gamma) \frac{\partial J}{\partial Q_{v_j,e}^{(t-1)}} \quad (16)$$

$$Q_{v_j,e}^{(t)} = Q_{v_j,e}^{(t-1)} - \alpha g_{v_j,e}^{(t)} \quad (17)$$

Variable node update

$$m_{v_j \rightarrow c_i}^{(t)} = Q_{v_j,e}^{(t)} - \langle e, H_{ij} \rangle m_{c_i \rightarrow v_j}^{(t)} \quad (18)$$

**Hard decision:**

**for**  $j = 1 \rightarrow N$ ,  $e \in \{X, Y, Z\}$ , **do**

**if**  $Q_{v_j,e}^{(t)} > 0$  for all  $e$ , **let**  $\hat{E}_i = I$

**else**, **let**  $\hat{E}_i = \arg \min_{e \in \{X, Y, Z\}} Q_{v_j,e}^{(t)}$

**if**  $\langle H, \hat{E} \rangle = s$ , **return** "converge" and halt.

**else if**  $t = iter_{max}$ , **return** "fail" and halt.

**else** repeat from **serial update**.

For the gradient calculation, we ignore the coefficient terms in Eq. (11), using the difference between the posterior updates calculated by traditional BP and the *a posteriori* probabilities from the previous iteration as the gradient for the current iteration, expanded in Eq. (19). When  $\alpha = 1$  and  $\gamma = 0$ , Eq. (19) is equivalent to the traditional BP's *a posteriori* update; when  $0 < \alpha < 1$  and  $\gamma = 0$ , it is equivalent to the EWA of *a posteriori* updates so far. In practice, to avoid the malice of hyper-parameter tuning and to enhance the interpretability of the formula, we can either fix  $\alpha$  at 1 or  $\gamma$  at 0.

$$Q_{v_j,e}^{(t)} = Q_{v_j,e}^{(t-1)} - \alpha \left( \gamma g_{v_j,e}^{(t-1)} + (1-\gamma)(Q_{v_j,e}^{(t-1)} - Q_{v_j,e}^{(0)} - \sum_{\substack{c_i \in \mathcal{M}(v_j) \\ \langle e, H_{ij} \rangle = 1}} m_{c_i \rightarrow v_j}^{(t)}) \right) \quad (19)$$

$$\stackrel{\text{if } \alpha=1}{=} \gamma(Q_{v_j,e}^{(t-1)} - g_{v_j,e}^{(t-1)}) + (1-\gamma)(Q_{v_j,e}^{(0)} + \sum_{\substack{c_i \in \mathcal{M}(v_j) \\ \langle e, H_{ij} \rangle = 1}} m_{c_i \rightarrow v_j}^{(t)}). \quad (20)$$

The properties of Momentum-BP can be explained from two perspectives. (1) Since it takes into account message updates from previous iterations, the method smooths the update direction in each iteration, preventing the corresponding energy function from oscillating between two points and gradually converging to the global minimum between them. (2) Node-wise momentum updates gradually break the symmetry of messages in the trapping sets shown in Fig. 2, allowing BP to escape from these trapping sets. The trapping set simulation in Section 4.1 will support those explanations.

### 3.1.2 Adaptive step size

The oscillation of message updates in trapping sets can also be attributed to the step size. In traditional LLR-BP, all variable node posterior updates result from directly accumulating messages from neighboring check nodes, which can become symmetric and cause oscillations. From the gradient perspective, if the step size is too large, the optimization algorithm is likely to oscillate; if the step size is too small, the algorithm is unable to update effectively. In practical decoding, the update frequency of different variable nodes may be uneven, with some requiring more rapid updates while others need to remain stable.

Inspired by adaptive gradient methods in deep learning, we propose AdaGrad-BP. The framework of this algorithm is very similar to Momentum-BP, with initialization and horizontal updates identical to traditional BP, while the posterior probability updates follow an adaptive step size rule, expressed as

$$Q_{v_j,e}^{(t)} = Q_{v_j,e}^{(t-1)} - \alpha \frac{g_{v_j,e}^{(t)}}{\sqrt{G_{v_j,e}^{(t)}} + \epsilon}, \quad (21)$$

where  $g_{v_j,e}^{(t)}$  approximates the gradient of the energy function

$$g_{v_j,e}^{(t)} = Q_{j,e}^{(t-1)} - Q_{j,e}^{(0)} - \sum_{\substack{c_i \in \mathcal{M}(v_j) \\ \langle e, H_{ij} \rangle = 1}} m_{c_i \rightarrow v_j}^{(t)}, \quad (22)$$

and  $G_{v_j,e}^{(t)}$  is the cumulative sum of the squared gradients as

$$G_{v_j,e}^{(t)} = G_{v_j,e}^{(t-1)} + (g_{v_j,e}^{(t)})^2. \quad (23)$$

This method adaptively alters the step size by accumulating historical gradient information. For instance, when the estimate of a variable node for a certain Pauli error changes significantly, the algorithm reduces the step size to counteract oscillation. Eq. (21) takes effect after the first iteration to ensure initial update stability. Here,  $\alpha$  is the boost learning rate, providing an update impetus as the algorithm begins to accumulate gradients. This learning rate is relatively insensitive; a moderate value suffices. In all our tests,  $\eta$  is fixed at 5. While AdaGrad-BP may face issues with accumulated gradients causing the step size to approach zero after many iterations, this does not significantly impact the algorithm. In practice, AdaGrad can reduce the number of iterations, allowing most error patterns to converge before the gradients become too small.

Regrettably, combining Momentum-BP and AdaGrad-BP using the Adam optimizer or other methods has not yielded satisfactory results. On one hand, the Adam algorithm introduces additional hyperparameters whose optimal values for BP decoding cannot be directly borrowed from deep learning, thereby complicating the algorithm. On the other hand, Momentum and AdaGrad approach similar message update optimizations from different perspectives, and a straightforward combination of the two can lead to overcompensation.

### 3.2 Dynamic Initial probability

BP decoding and gradient descent still have a fundamental difference, which limits the performance of algorithms in Section 3.1. Each update in gradient descent is based on the previous step's results, whereas in BP decoding, each calculation of *a posteriori* probabilities accumulates the same *a priori* probabilities. Given the objective function as shown in Eq. (2), for simplicity using the binary domain for instance, BP calculates the LLR values as

$$Q_{v_j} = \ln \frac{P(e_j = 0|s)}{P(e_j = 1|s)} \quad (24)$$

$$= \ln \frac{P(e_j = 0) \cdot P(s|e_j = 0)}{P(e_j = 1) \cdot P(s|e_j = 1)} \quad (25)$$

$$= Q_{v_j}^{(0)} + \sum_{c_{i'} \in \mathcal{M}(v_j) \setminus c_i} m_{c_{i'} \rightarrow v_j}, \quad (26)$$

where  $Q_{v_j}^{(0)}$  is a manually set initial value of the algorithm that participates in each iteration's *a posteriori* probability update. However, since the prior error probabilities are derived from an theoretical channel which is hard to measure and estimate in experiments, the *a priori* probabilities can significantly affect the BP iterations.

Existing methods for altering initial probabilities include re-initialization using information obtained from previous iterations [20, 21, 30], as well as detecting oscillations during the decoding process and modifying initial values accordingly [31]. However, they either require multiple outer loops or manually set algorithm parameters. This subsection introduces two methods for dynamically updating initial values, utilizing *a posteriori* probabilities from previous iterations to accelerate the convergence of BP decoding with almost no additional overhead.

#### 3.2.1 EWA Initialization

The first method employs a transformed exponential weighted averaging, incorporating components of all previous *a posteriori* probabilities into the *a priori* probabilities with a decaying factor. EWAInit-BP under parallel scheduling is shown in algorithm 2.

In fact, combining Eq. (27) and Eq. (8), EWAInit-BP exhibits similar characteristics to Momentum-BP, namely the exponentially decaying components of previous iterations. The difference is that the former aggressively changes the

---

**Algorithm2** EWAInit-BP under Parallel Scheduling for Quaternary Log Domain

---

**Input:** Parity-check matrix  $\mathbf{H}$ , syndrome vector  $\mathbf{s}$ , *a priori* LLR vectors  $Q^{(0)}$ , max iterations  $iter_{max}$ , discount factor  $\alpha$ .

**Output:** Estimated error vector  $\hat{\mathbf{E}}$ .

**EWA Initialization:**

**for**  $j = 1 \rightarrow N$ ,  $e \in \{X, Y, Z\}$ , **do**

$$\Pi_{v_j, e}^{(t)} = \alpha Q_{v_j, e}^{(0)} + (1 - \alpha) Q_{v_j, e}^{(t-1)} \quad (27)$$

**Horizontal update:**

**for**  $i = 1 \rightarrow M$ , calculate  $m_{c_i \rightarrow v_j}^{(t)}$  as Eq. (5)

**Vertical update:**

**for**  $j = 1 \rightarrow N$ , calculate  $m_{v_j \rightarrow c_i}^{(t)}$  as Eq. (7)

**Hard decision:**

**for**  $j = 1 \rightarrow N$ ,  $e \in \{X, Y, Z\}$ , **do**

Calculate  $Q_{v_j, e}^{(t)}$  as Eq. (8)

**if**  $Q_{v_j, e}^{(t)} > 0$  for all  $e$ , **let**  $\hat{E}_i = I$

**else**, **let**  $\hat{E}_i = \arg \min_{e \in \{X, Y, Z\}} Q_{v_j, e}^{(t)}$

**if**  $\langle \mathbf{H}, \hat{\mathbf{E}} \rangle = \mathbf{s}$ , **return** "converge" and halt.

**else if**  $t = iter_{max}$ , **return** "fail" and halt.

**else** repeat from **EWA Initialization**.

---

"prior" probability of each variable node in each iteration. Eq. (27) still retains a portion of the input prior probabilities. In our experiments, we tried replacing this term with the prior probabilities from the previous iteration, but the algorithm's performance did not significantly change.

#### 3.2.2 Adaptive Initialization

The second method is similar to the AdaGrad approach used in message updates, except that it updates the prior probabilities, shown as

$$g_{v_j, e}^{(t)} = Q_{v_j, e}^{(t-1)} - Q_{v_j, e}^{(0)} \quad (28)$$

$$G_{v_j, e}^{(t)} = G_{v_j, e}^{(t-1)} + (g_{v_j, e}^{(t)})^2 \quad (29)$$

$$\Pi_{v_j, e}^{(t)} = Q_{v_j, e}^{(0)} + \frac{\alpha g_{v_j, e}^{(t)}}{\sqrt{G_{v_j, e}^{(t)} + \epsilon}} \quad (30)$$

The core concept involves calculating the difference between the *a posteriori* probabilities from the previous iteration and the initial *a priori* probability, and updating this difference with a decayed learning rate.

### 3.3 Complexity

Our proposed algorithms involve the same message passing between variable nodes and check nodes as traditional BP. The main difference lies in the additional update steps, which in Momentum-BP and AdaGrad-BP consist of recalculating the *a posteriori* probabilities, and in EWAInit-BP and AdaInit-BP involve recalculating the initial values. These additional steps only involve simple arithmetic operations and can be executed locally at each node, without requiring extra iterations, loops, or global communication, thus not introducing any significant overhead. Therefore, the overall time complexity of the proposed algorithms remains  $O(j\tau N)$ , where  $j$  is the average degree of the Tanner graph, and  $\tau$  is the number of iterations.

In terms of space complexity, traditional BP requires storing messages and probability values, resulting in  $O(N)$  space requirements. Our algorithms only add extra storage space to accumulate gradients or maintain exponential weighted averages which is proportional to the number of variable nodes and does not change the overall space complexity. Thus, our improved algorithms maintain the same efficiency in both time and space as traditional BP, ensuring scalability and feasibility for practical implementation.

## 4 Simulation Results

In all simulations, the criterion for successful decoding is that the error estimate satisfies  $\hat{E} \in E\mathcal{S}$ , rather than  $\hat{E} = E$  as in classical information. All cases not meeting the above condition are referred to as *logical errors* in this paper. Herein, a *detected error* refers to  $\hat{E}E$  being anti-commutative with any one stabilizer  $S \in \mathcal{S}$ ; an *undetected error* implies  $\hat{E}E$  commutes with all stabilizers, i.e.,  $\hat{E}E \in N(\mathcal{S}) \setminus \mathcal{S}$ , where the result of error correction is a logical operator. Each data point on the experimental curves represents the mean of at least  $10^4$  simulations.

Our simulations employ a depolarizing channel, where each qubit has an equal probability  $p/3$  of experiencing X, Y, or Z Pauli errors, and a probability of  $1 - p$  of no error occurring. Additionally, for ease of comparison, we adopt the simple noise model which does not consider measurement errors or error propagation in quantum circuits.

### 4.1 Breaking the Trapping Sets

We first compare the performance of improved BP on the trapping set shown in Fig. 2. In this example, qubit 1 and qubit 2 experience X errors, resulting in an error syndrome of [1,0,1,0]. Fig. 3 shows the comparison between the traditional LLR-BP<sub>4</sub>, Momentum-BP and AdaGrad-BP in Section 3.1 *under parallel scheduling*, with the maximum iteration set to 50. The hard decision result of the traditional BP oscillates continuously between all X and all I, while the improved BP shows significantly reduced oscillation amplitude and converges within 12 iterations.

A more detailed comparison of the different algorithms proposed in this paper is presented in Table 1. The parameters used for the algorithms are defaults and were not specially optimized for this example. MBP [25] converges at the same fastest speed under serial scheduling but oscillates under parallel scheduling. BP-OTS [31] shows little dependency on scheduling method but its convergence depends on the manually set oscillation period  $T$ , which may vary in different error correction scenarios. The algorithms proposed in Section 3.1, Momentum-BP and AdaGrad-BP, both converge under parallel scheduling. Besides, AdaGrad-BP and EWAInit-BP with adaptive *a priori* probabilities converge at the fastest speed under serial scheduling.

### 4.2 BP Optimization on Topological codes

In this subsection, we compare the performance of the various BP optimization proposed in this paper. Subsequently, we present comparisons of our algorithm with other BP improvements without post-processing on Toric codes, Surface codes, and XZZX Surface codes. For all decoding algorithms, the maximum number of iterations  $iter_{max}$  across all code lengths is set to 150 to ensure linear asymptotic complexity.

#### 4.2.1 Comparison of our BP optimization methods

A comparison of all methods proposed in this paper is illustrated in Fig. 4. The two methods for optimizing message update rules, Momentum-BP and AdaGrad-BP, exhibit some improvements over traditional BP at low physical error rates, while their performance gradually converging to that of traditional BP as the physical error rate

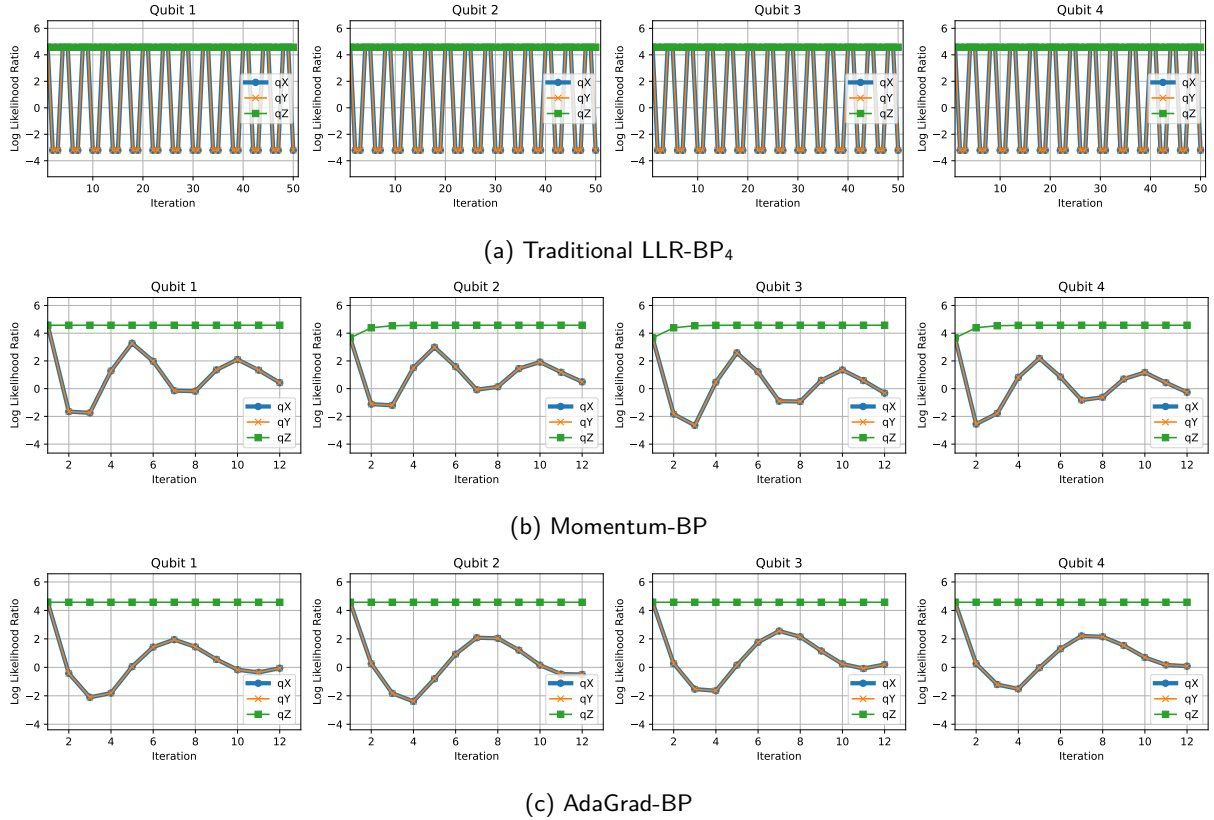


Figure 3: Comparison of traditional LLR-BP<sub>4</sub>, Momentum-BP, and AdaGrad-BP under parallel scheduling on the (4,0) trapping set. The latter two methods break the symmetry of message updates and converge within 12 iterations.

Table 1: Iterations required by different BP algorithms on the (4,0) trapping set

Algorithm	Parallel Scheduling	Serial Scheduling
LLR-BP <sub>4</sub> [28]	—	—
MBP [25] ( $\alpha = 0.6$ )	—	2 iterations
BP-OTS [31] (Different T)	T+2 iterations	T+2 iterations
Momentum-BP( $\alpha = 0.6$ )	12 iterations	6 iterations
<b>AdaGrad-BP(<math>\alpha = 5</math>)</b>	<b>12 iterations</b>	<b>2 iterations</b>
EWAInit-BP( $\alpha = 0.6$ )	—	2 iterations

increases. The two methods for optimizing initial values, AdaInit-BP and EWAInit-BP, demonstrate improvements ranging from 1 to 4 orders of magnitude over traditional BP, and excellently eliminate the error floor. However, the performance of algorithms that combine these two ideas is not satisfactory, because both approaches inherently consider the historical *a posteriori* probabilities but from different positions within the BP algorithm. This two methods are essentially addressing the same problem—incorporating past information to refine current updates. As a result, simply merging them can lead to redundancy and overcompensation, which negatively impacts the overall performance.

#### 4.2.2 Toric code

We construct the  $[[2n^2, 1, n]]$  toric code based on its properties as a hypergraph product of an  $[n, 1]$  repetition code. The toric code features periodic boundaries, hence all its stabilizers have a weight of four, and any error syndromes on it exhibit translational symmetry [50], which is particularly conducive to BP and neural network decoding. We compare the performance of our EWAInit-BP and other existing methods under both parallel and serial scheduling as shown in Fig. 5 and Fig. 6, respectively.

For the parallel schedule, compared to the classic logarithmic domain quaternary BP and its en-

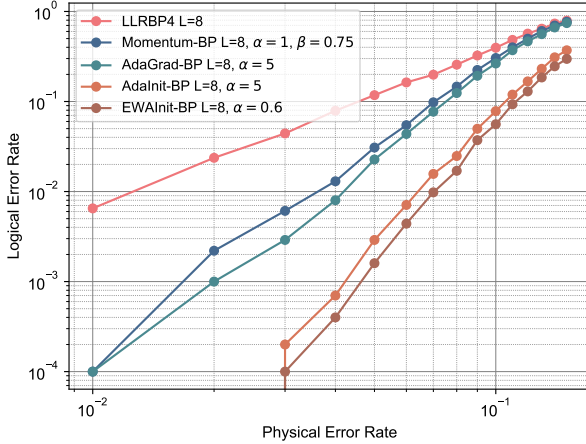
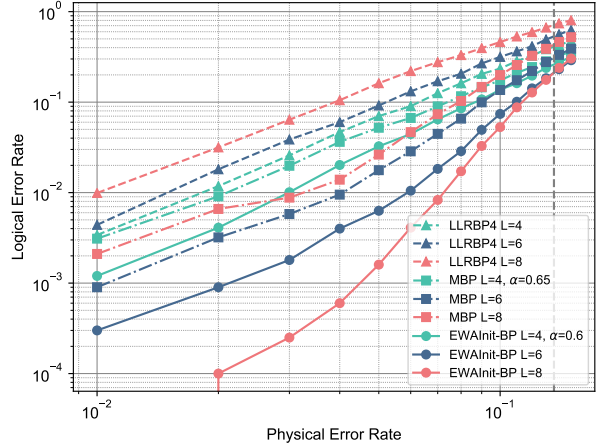


Figure 4: Performance of various BP optimization methods presented in this paper, demonstrated using the  $L = 8$  toric code as an example. Each method uses default parameters and has not been optimized for this specific case. Among these, the method for optimizing initial values, EWAInit-BP, exhibits the best performance and completely eliminates the error floor.

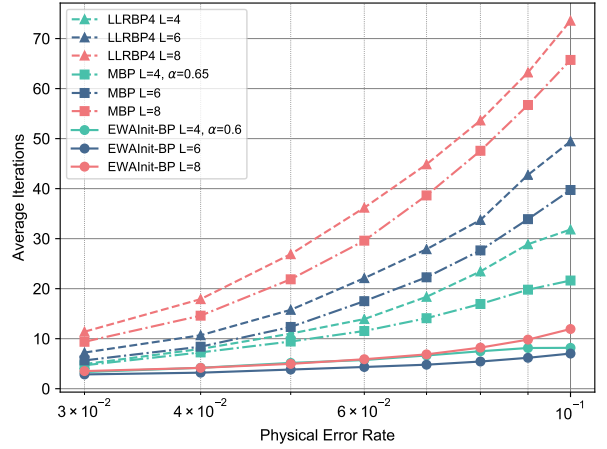
hancement, MBP, our EWAInit-BP is the only method that achieves a decrease in logical error rates as the lattice size increases, with significant improvements in logical error rates at the same lattice size.<sup>1</sup> The intersection of the error rate curves for these lattice sizes is approximately 13.6%. Additionally, the average number of iterations required for EWAInit-BP is significantly lower than the other two methods, converging in fewer than 10 iterations mostly. Parallel scheduling of BP algorithms holds the potential to achieve constant complexity through hardware-based parallel computation, while EWAInit-BP ensures both the error correction capabilities and speed in decoding.

For the serial schedule, all three decoding algorithms demonstrated error correction capabilities. Among those, BP-OTS performs better than MBP at low physical error rates, but its performance is surpassed by MBP when the physical error rate exceeds 7%. The performance of EWAInit-BP, on the other hand, consistently outperforms these two methods across all tested conditions, with the logical error rate at  $L = 6$  being comparable to that of the other two algorithms at  $L = 8$ , and the intersection of the logical er-

<sup>1</sup>Our implementation of BP-OTS in the quaternary domain with parallel scheduling did not achieve the performance reported in the original paper, necessitating further investigation into this discrepancy.



(a) Logical error rates

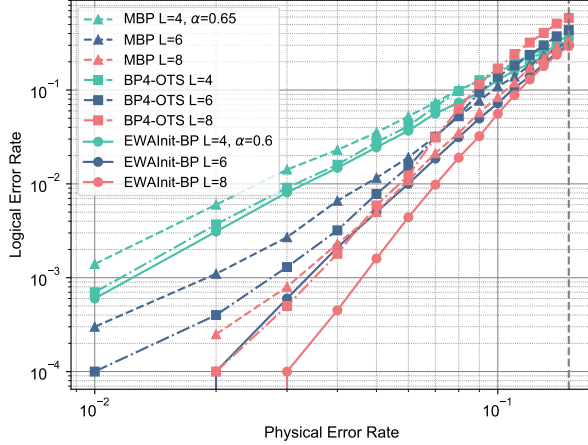


(b) Average iterations

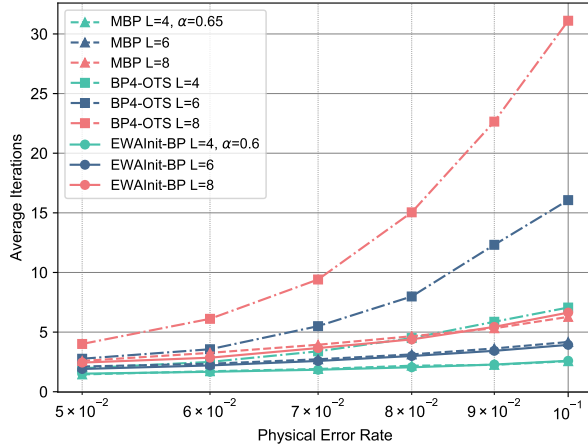
Figure 5: Performance of LLRBP4, MBP, and EWAInit-BP under parallel scheduling on toric codes with lattice sizes of 4, 6, 8. Only EWAInit-BP demonstrates a reduction in the logical error rate as the lattice size increases, with the intersection of error rates occurring at 13.6%.

ror rate curves is approximately 15%. In terms of iteration count, both EWAInit-BP and MBP converge in remarkably few iterations (often fewer than 5).

It is noteworthy that for the toric code, the performance of EWAInit-BP under parallel scheduling is not significantly different from serial scheduling. This is due to the method's inherent ability to effectively break trapping sets, combined with the geometric symmetry of the Toric code, which allows for less dependency on the scheduling method. However, for the following topological codes with more complex stabilizer configurations, serial scheduling shows better performance.



(a) Logical error rates



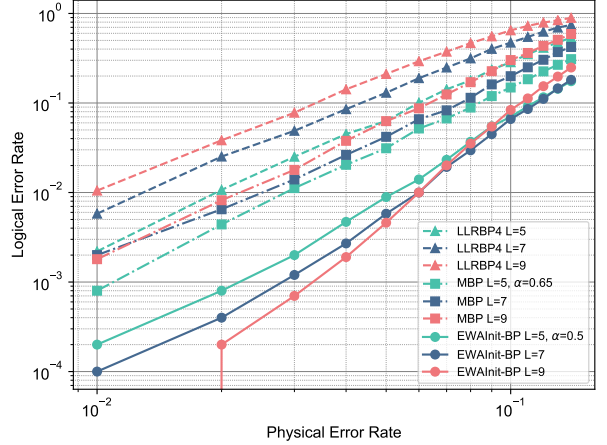
(b) Average iterations

Figure 6: Performance of MBP, BP-OTS, and EWAInit-BP under serial scheduling on toric codes with  $L = 4, 6, 8$ . We choose  $T = 9$  and  $C = 20$  for BP-OTS. EWAInit-BP outperforms other BP improvements, with the intersection of logical error rates at 15%.

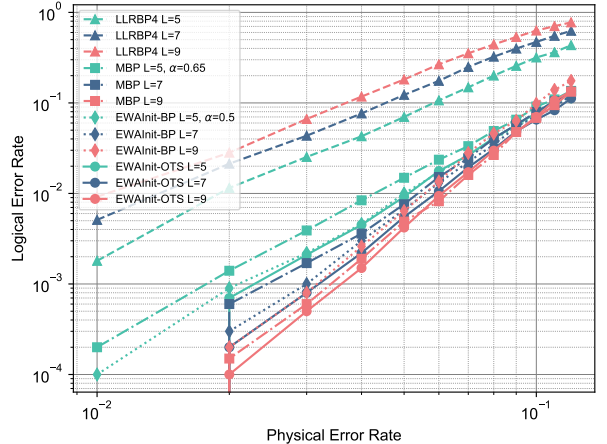
#### 4.2.3 Planar surface code

The boundaries of the planar surface code are no longer contiguous, resulting in the emergence of some stabilizers with weight three and qubits that only connect two stabilizers at the boundaries. This configuration leads to a slight reduction in the error correction capabilities of the planar surface code compared to the Toric code. We compare the decoding logical error rates of LLRBP4, MBP, and EWAInit-BP under both parallel and serial scheduling, as illustrated in Fig. 7.

Under parallel scheduling, the decoding logical error rates of LLRBP4 and MBP4 increase with increasing code length, while EWAInit-BP achieves a reduction in logical error rates at low



(a) LER under a parallel schedule



(b) LER under a serial schedule

Figure 7: Performance of LLRBP4, MBP, and EWAInit-BP (EWAInit-OTS) on planar surface codes with  $L = 5, 7, 9$ . The intersection of logical error rates for EWAInit-BP under serial scheduling is approximately 10%.

physical error rates. Unfortunately, at higher error rates, decoding at higher code lengths becomes more challenging, preventing EWAInit-BP from achieving a reliable threshold on the planar surface code.

Under serial scheduling, EWAInit-BP performs better than MBP at  $L = 5$  and  $L = 7$ ; however, its performance at  $L = 9$  is not satisfying. In fact, the decoding failure rate of EWAInit-BP increases with higher code lengths, thus not fully demonstrating the error-correcting capabilities of the code. This is because, despite the dynamic updating of *a priori* probabilities, the method still partly relies on the initial input priors. We incorporate the OTS method as a "post-processing" step for EWAInit, resetting the *a priori* probabilities of some nodes every few iter-

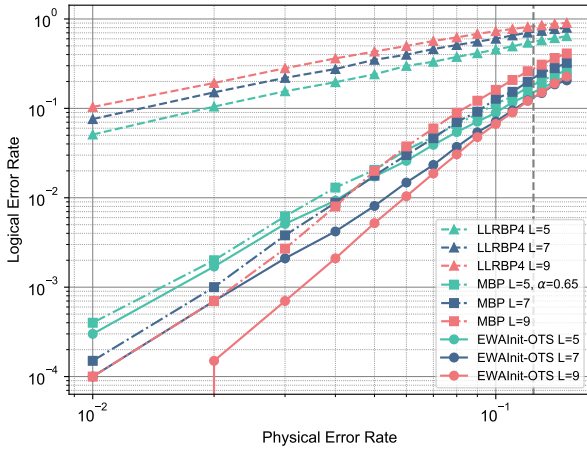


Figure 8: Performance of LLRBP4, MBP, and EWAInit-BP (EWAInit-OTS) on XZZX surface codes with  $L = 5, 7, 9$  under serial scheduling. The intersection of logical error rates for EWAInit-BP is approximately 12.4%.

ations. We choose parameter  $T=5$  and  $C=20$ . This EWAInit-OTS method, while maintaining a time complexity of  $O(n)$ , shows improvements in convergence rate and logical error rates on the surface code compared to EWAInit-BP.

#### 4.2.4 XZZX Surface code

For biased noise, the XZZX surface code exhibits superior error correction capabilities compared to the traditional planar surface code, achieving the theoretical maximum threshold of 50% across three types of pure Pauli error channels.

A comparison of decoding performance on the XZZX surface code is illustrated in Fig. 8. Our EWAInit combined with OTS method outperforms other algorithms under serial scheduling, with the LER curve intersection at approximately 12.4%. Unfortunately, for odd lattice sizes, the logical error rate for higher code lengths is higher than for lower code lengths at low physical error rates, while it demonstrates error-correcting capabilities at higher physical error rates.

To demonstrate the bias noise correction capability of the XZZX surface code, we chose  $p_z = \frac{2}{3}$  and  $p_x = p_y = \frac{1}{6}$ , implying that Pauli Z errors are more likely to occur, which aligns with the conditions found in actual hardware. Fig. 9 displays the decoding performance under biased noises under parallel scheduling. It is evident that when biased noise is present, the performance of BP decoding using the XZZX surface code with parallel scheduling shows significant improvement

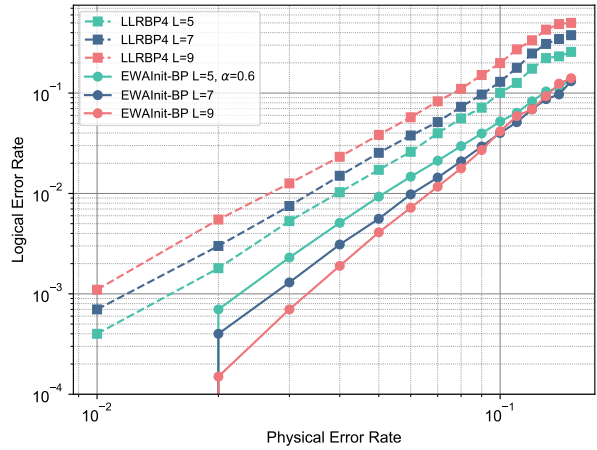


Figure 9: Performance of LLRBP4 and EWAInit-BP on the XZZX surface code with  $L = 5, 7, 9$  under parallel scheduling, evaluated under conditions where Pauli Z errors are more prevalent in the channel. The intersection of LERs for EWAInit-BP is approximately 10%.

compared to that on a depolarizing channel. Besides, EWAInit-BP offers an improvement of approximately one order of magnitude and demonstrates the error correction capability under parallel scheduling, with the intersection of logical error rates around 10%.

## 5 Summary

We analyzed the reasons for BP’s poor performance on surface codes, namely trapping sets formed by 8-cycles and symmetric degeneracy. In these trapping sets, the probability vectors in each iteration exhibit periodic oscillations. We proposed several methods to mitigate this issue.

Since the *a posteriori* probability update of BP can be interpreted as the gradient optimization of an energy function, we borrowed optimization strategies from gradient descent in machine learning, proposing Momentum-BP and AdaGrad-BP. These mechanisms aim to smooth the update direction and reduce the amplitude of oscillations, respectively. Experiments on trapping sets intuitively demonstrated the effectiveness of these algorithms.

From the theoretical derivation of the BP algorithm, we identified the importance of *a priori* probabilities and transformed the message update smoothing into initial values adapting, proposing EWAInit-BP. This algorithm exhibits aggressive exploration and outperforms state-of-

the-art algorithms without OSD post-processing on the Toric code, Surface code, and XZZX Surface code. Specifically, EWAInit-BP can demonstrate error correction capabilities even under parallel scheduling, with logical error rates decreasing as code length increases. Notably, all our proposed methods do not introduce any additional factors to the time complexity of BP. Thus, EWAInit-BP can be implemented with  $O(1)$  complexity in fully parallel while maintaining decoding accuracy.

Parameterized BP algorithms involve a trade-off between convergence and the occurrence of logical operators. Our methods primarily focus on ensuring convergence, as the main issue with BP on surface codes lies in achieving this, which subsequently leads to an increased rate of logical operators. Therefore, it is challenging to apply our improvements directly to general quantum error-correcting codes. A potential research direction is to use AI methods to explore this trade-off and find the optimal balance for the lowest error rate.

Additionally, our simulations only considered Pauli errors on qubits and did not account for measurement errors, error propagation in circuits, etc. Future work needs to adapt BP to more challenging noise models, potentially requiring specialized optimizations.

## References

[1] Ye Wang, Mark Um, Junhua Zhang, Shuoming An, Ming Lyu, Jing-Ning Zhang, L-M Duan, Dahyun Yum, and Kihwan Kim. Single-qubit quantum memory exceeding ten-minute coherence time. *Nature Photonics*, 11(10):646–650, 2017. DOI: [10.1038/s41566-017-0007-1](https://doi.org/10.1038/s41566-017-0007-1).

[2] P.W. Shor. Fault-tolerant quantum computation. In *Proceedings of 37th Conference on Foundations of Computer Science*, pages 56–65, 1996. DOI: [10.1109/SFCS.1996.548464](https://doi.org/10.1109/SFCS.1996.548464).

[3] Daniel Gottesman. *Stabilizer codes and quantum error correction*. California Institute of Technology, 1997.

[4] H. Bombin. An introduction to topological quantum codes. 2013. DOI: [10.48550/arXiv.1311.0277](https://doi.org/10.48550/arXiv.1311.0277).

[5] Rami Barends, Julian Kelly, Anthony Megrant, Andrzej Veitia, Daniel Sank, Evan Jeffrey, Ted C White, Josh Mutus, Austin G Fowler, Brooks Campbell, et al. Superconducting quantum circuits at the surface code threshold for fault tolerance. *Nature*, 508(7497):500–503, 2014. DOI: [10.1038/nature13171](https://doi.org/10.1038/nature13171).

[6] Youwei Zhao, Yangsen Ye, He-Liang Huang, Yiming Zhang, Dachao Wu, Huijie Guan, Qingling Zhu, Zuolin Wei, Tan He, Sirui Cao, Fusheng Chen, Tung-Hsun Chung, Hui Deng, Daojin Fan, Ming Gong, Cheng Guo, Shaojun Guo, Lianchen Han, Na Li, Shaowei Li, Yuan Li, Futian Liang, Jin Lin, Haoran Qian, Hao Rong, Hong Su, Lihua Sun, Shiyu Wang, Yulin Wu, Yu Xu, Chong Ying, Jiale Yu, Chen Zha, Kaili Zhang, Yong-Heng Huo, Chao-Yang Lu, Cheng-Zhi Peng, Xiaobo Zhu, and Jian-Wei Pan. Realization of an error-correcting surface code with superconducting qubits. *Phys. Rev. Lett.*, 129:030501, Jul 2022. DOI: [10.1103/PhysRevLett.129.030501](https://doi.org/10.1103/PhysRevLett.129.030501).

[7] Google Quantum AI. Suppressing quantum errors by scaling a surface code logical qubit. *Nature*, 614(7949):676–681, 2023. DOI: [10.1038/s41586-022-05434-1](https://doi.org/10.1038/s41586-022-05434-1).

[8] Robert Raussendorf and Jim Harrington. Fault-tolerant quantum computation with high threshold in two dimensions. *Physical review letters*, 98(19):190504, 2007. DOI: [10.1103/PhysRevLett.98.190504](https://doi.org/10.1103/PhysRevLett.98.190504).

[9] Austin G. Fowler, Matteo Mariantoni, John M. Martinis, and Andrew N. Cleland. Surface codes: Towards practical large-scale quantum computation. *Physical Review A*, Sep 2012. DOI: [10.1103/physreva.86.032324](https://doi.org/10.1103/physreva.86.032324).

[10] A Yu Kitaev. Fault-tolerant quantum computation by anyons. *Annals of physics*, 303(1):2–30, 2003. DOI: [10.1016/S0003-4916\(02\)00018-0](https://doi.org/10.1016/S0003-4916(02)00018-0).

[11] J. Pablo Bonilla Ataides, David K. Tuckett, Stephen D. Bartlett, Steven T. Flammia, and Benjamin J. Brown. The xzzx surface code. *Nature Communications*, Apr 2021. DOI: [10.1038/s41467-021-22274-1](https://doi.org/10.1038/s41467-021-22274-1).

[12] Jack Edmonds. Paths, trees, and flowers. *Canadian Journal of mathematics*, 17:449–467, 1965. DOI: [10.4153/CJM-1965-045-4](https://doi.org/10.4153/CJM-1965-045-4).

[13] Sergey Bravyi, Martin Suchara, and Alexander Vargo. Efficient algorithms for maximum likelihood decoding in the surface code.

*Phys. Rev. A*, 90:032326, Sep 2014. DOI: [10.1103/PhysRevA.90.032326](https://doi.org/10.1103/PhysRevA.90.032326).

[14] Guillaume Duclos-Cianci and David Poulin. Fast decoders for topological quantum codes. *Physical Review Letters*, Mar 2010. DOI: [10.1103/physrevlett.104.050504](https://doi.org/10.1103/physrevlett.104.050504).

[15] Nicolas Delfosse, Vivien Londe, and Michael E. Beverland. Toward a union-find decoder for quantum ldpc codes. *IEEE Transactions on Information Theory*, 68(5):3187–3199, 2022. DOI: [10.1109/TIT.2022.3143452](https://doi.org/10.1109/TIT.2022.3143452).

[16] Adam Holmes, Mohammad Reza Jokar, Ghasem Pasandi, Yongshan Ding, Massoud Pedram, and Frederic T. Chong. Nisq+: Boosting quantum computing power by approximating quantum error correction. In *2020 ACM/IEEE 47th Annual International Symposium on Computer Architecture (ISCA)*, pages 556–569, 2020. DOI: [10.1109/ISCA45697.2020.00053](https://doi.org/10.1109/ISCA45697.2020.00053).

[17] Francesco Battistel, Christopher Chamberland, Kauser Johar, Ramon WJ Overwater, Fabio Sebastiano, Luka Skoric, Yosuke Ueno, and Muhammad Usman. Real-time decoding for fault-tolerant quantum computing: Progress, challenges and outlook. *Nano Futures*, 7(3):032003, 2023. DOI: [10.1088/2399-1984/aceba6](https://doi.org/10.1088/2399-1984/aceba6).

[18] D.J.C. MacKay, G. Mitchison, and P.L. McFadden. Sparse-graph codes for quantum error correction. *IEEE Transactions on Information Theory*, 50(10):2315–2330, 2004. DOI: [10.1109/TIT.2004.834737](https://doi.org/10.1109/TIT.2004.834737).

[19] Javier Valls, Francisco Garcia-Herrero, Nithin Raveendran, and Bane Vasić. Syndrome-based min-sum vs osd-0 decoders: Fpga implementation and analysis for quantum ldpc codes. *IEEE Access*, 9: 138734–138743, 2021. DOI: [10.1109/ACCESS.2021.3118544](https://doi.org/10.1109/ACCESS.2021.3118544).

[20] David Poulin and Yeojin Chung. On the iterative decoding of sparse quantum codes. 2008. DOI: [10.48550/arXiv.0801.1241](https://doi.org/10.48550/arXiv.0801.1241).

[21] Yun-Jiang Wang, Barry C. Sanders, Bao-Ming Bai, and Xin-Mei Wang. Enhanced feedback iterative decoding of sparse quantum codes. *IEEE Transactions on Information Theory*, page 1231–1241, Feb 2012. DOI: [10.1109/tit.2011.2169534](https://doi.org/10.1109/tit.2011.2169534).

[22] Zunaira Babar, Panagiotis Botsinis, Dimitrios Alanis, Soon Xin Ng, and Lajos Hanzo. Fifteen years of quantum ldpc coding and improved decoding strategies. *IEEE Access*, page 2492–2519, Jan 2015. DOI: [10.1109/ACCESS.2015.2503267](https://doi.org/10.1109/ACCESS.2015.2503267).

[23] Nithin Raveendran, Mohsen Bahrami, and Bane Vasic. Syndrome-generalized belief propagation decoding for quantum memories. In *ICC 2019 - 2019 IEEE International Conference on Communications (ICC)*, May 2019. DOI: [10.1109/icc.2019.8761366](https://doi.org/10.1109/icc.2019.8761366).

[24] Kao-Yueh Kuo and Ching-Yi Lai. Refined belief propagation decoding of sparse-graph quantum codes. *IEEE Journal on Selected Areas in Information Theory*, page 487–498, Aug 2020. DOI: [10.1109/jsait.2020.3011758](https://doi.org/10.1109/jsait.2020.3011758). URL <http://dx.doi.org/10.1109/jsait.2020.3011758>.

[25] Kao-Yueh Kuo and Ching-Yi Lai. Exploiting degeneracy in belief propagation decoding of quantum codes. *npj Quantum Information, npj Quantum Information*, Apr 2021. DOI: [10.1038/s41534-022-00623-2](https://doi.org/10.1038/s41534-022-00623-2).

[26] Kao-Yueh Kuo and Ching-Yi Lai. Comparison of 2d topological codes and their decoding performances. In *2022 IEEE International Symposium on Information Theory (ISIT)*, pages 186–191, 2022. DOI: [10.1109/ISIT50566.2022.9834489](https://doi.org/10.1109/ISIT50566.2022.9834489).

[27] Alex Rigby, J. C. Olivier, and Peter Jarvis. Modified belief propagation decoders for quantum low-density parity-check codes. *Physical Review A*, Jul 2019. DOI: [10.1103/physreva.100.012330](https://doi.org/10.1103/physreva.100.012330).

[28] Ching-Yi Lai and Kao-Yueh Kuo. Log-domain decoding of quantum ldpc codes over binary finite fields. *IEEE Transactions on Quantum Engineering*, 2:1–15, 2021. DOI: [10.1109/TQE.2021.3113936](https://doi.org/10.1109/TQE.2021.3113936).

[29] Zhengzhong Yi, Zhipeng Liang, Kaixin Zhong, Yulin Wu, Zhou Fang, and Xuan Wang. Improved belief propagation decoding algorithm based on decoupling representation of pauli operators for quantum ldpc codes. *arXiv preprint arXiv:2305.17505*, 2023. DOI: [10.48550/arXiv.2305.17505](https://doi.org/10.48550/arXiv.2305.17505).

[30] Josias Old and Manuel Rispler. Generalized belief propagation algorithms for decoding of surface codes. *Quantum*, 7:1037, 2023. DOI: [10.22331/q-2023-06-07-1037](https://doi.org/10.22331/q-2023-06-07-1037).

[31] Dimitris Chytas, Michele Pacenti, Nithin

Raveendran, Mark F. Flanagan, and Bane Vasić. Enhanced message-passing decoding of degenerate quantum codes utilizing trapping set dynamics. *IEEE Communications Letters*, 28(3):444–448, 2024. DOI: [10.1109/LCOMM.2024.3356312](https://doi.org/10.1109/LCOMM.2024.3356312).

[32] Ben Criger and Imran Ashraf. Multipath summation for decoding 2d topological codes. *Quantum*, page 102, Oct 2018. DOI: [10.22331/q-2018-10-19-102](https://doi.org/10.22331/q-2018-10-19-102).

[33] Oscar Higgott, ThomasC. Bohdanowicz, Aleksander Kubica, StevenT. Flammia, and EarlT. Campbell. Improved decoding of circuit noise and fragile boundaries of tailored surface codes. *PRX Quantum*, Mar 2022. DOI: [10.1103/PhysRevX.13.031007](https://doi.org/10.1103/PhysRevX.13.031007).

[34] Laura Caune, Brendan Reid, Joan Camps, and Earl Campbell. Belief propagation as a partial decoder. 2023. DOI: [10.48550/arXiv.2306.17142](https://doi.org/10.48550/arXiv.2306.17142).

[35] Julien Du Crest, Mehdi Mhalla, and Valentin Savin. Stabilizer inactivation for message-passing decoding of quantum ldpc codes. In *2022 IEEE Information Theory Workshop (ITW)*, pages 488–493, 2022. DOI: [10.1109/ITW54588.2022.9965902](https://doi.org/10.1109/ITW54588.2022.9965902).

[36] Pavel Panteleev and Gleb Kalachev. Degenerate quantum ldpc codes with good finite length performance. *Quantum*, 5:585, 2021. DOI: [10.22331/q-2021-11-22-585](https://doi.org/10.22331/q-2021-11-22-585).

[37] Joschka Roffe, David R. White, Simon Burton, and Earl Campbell. Decoding across the quantum ldpc code landscape. *Physical Review Research*, Dec 2020. DOI: [10.1103/physrevresearch.2.043423](https://doi.org/10.1103/physrevresearch.2.043423).

[38] Sergey Bravyi, Andrew W Cross, Jay M Gambetta, Dmitri Maslov, Patrick Rall, and Theodore J Yoder. High-threshold and low-overhead fault-tolerant quantum memory. *Nature*, 627(8005):778–782, 2024. DOI: [10.1038/s41586-024-07107-7](https://doi.org/10.1038/s41586-024-07107-7).

[39] Ching-Feng Kung, Kao-Yueh Kuo, and Ching-Yi Lai. On belief propagation decoding of quantum codes with quaternary reliability statistics. In *2023 12th International Symposium on Topics in Coding (ISTC)*, pages 1–5, 2023. DOI: [10.1109/ISTC57237.2023.10273527](https://doi.org/10.1109/ISTC57237.2023.10273527).

[40] Patricio Fuentes, Josu Etxezarreta Martinez, Pedro M. Crespo, and Javier Garcia-Frías. Degeneracy and its impact on the decoding of sparse quantum codes. *IEEE Access*, 9:89093–89119, 2021. DOI: [10.1109/ACCESS.2021.3089829](https://doi.org/10.1109/ACCESS.2021.3089829).

[41] Nithin Raveendran and Bane Vasić. Trapping sets of quantum ldpc codes. *Quantum*, 5:562, 2021. DOI: [10.22331/q-2021-10-14-562](https://doi.org/10.22331/q-2021-10-14-562).

[42] Nikolas P. Breuckmann and Jens Niklas Eberhardt. Quantum low-density parity-check codes. *PRX Quantum*, Oct 2021. DOI: [10.1103/prxquantum.2.040101](https://doi.org/10.1103/prxquantum.2.040101).

[43] Min-Hsiu Hsieh and François Le Gall. Np-hardness of decoding quantum error-correction codes. *Physical Review A*, May 2011. DOI: [10.1103/physreva.83.052331](https://doi.org/10.1103/physreva.83.052331).

[44] D.E. Hocevar. A reduced complexity decoder architecture via layered decoding of ldpc codes. In *IEEE Workshop on Signal Processing Systems, 2004. SIPS 2004.*, Dec 2004. DOI: [10.1109/sips.2004.1363033](https://doi.org/10.1109/sips.2004.1363033).

[45] R. Lucas, M. Bossert, and M. Breitbach. On iterative soft-decision decoding of linear binary block codes and product codes. *IEEE Journal on Selected Areas in Communications*, page 276–296, Jan 1998. DOI: [10.1109/49.661116](https://doi.org/10.1109/49.661116).

[46] Mehdi Karimi Dehkordi and Amir H. Banihashemi. An efficient algorithm for finding dominant trapping sets of ldpc codes. In *2010 6th International Symposium on Turbo Codes; Iterative Information Processing*, Sep 2010. DOI: [10.1109/istc.2010.5613902](https://doi.org/10.1109/istc.2010.5613902).

[47] Seokju Han, Jieun Oh, Kyungmok Oh, and Jeongseok Ha. Deep-learning for breaking the trapping sets in low-density parity-check codes. *IEEE Transactions on Communications*, page 2909–2923, May 2022. DOI: [10.1109/tcomm.2022.3157314](https://doi.org/10.1109/tcomm.2022.3157314).

[48] Soonyoung Kang, Jaekyun Moon, Jeongseok Ha, and Jinwoo Shin. Breaking the trapping sets in ldpc codes: Check node removal and collaborative decoding. *IEEE Transactions on Communications*, 64(1):15–26, 2016. DOI: [10.1109/TCOMM.2015.2498161](https://doi.org/10.1109/TCOMM.2015.2498161).

[49] Asit Kumar Pradhan, Nithin Raveendran, Narayanan Rengaswamy, Xin Xiao, and Bane Vasić. Learning to decode trapping sets in qldpc codes. In *2023 12th International Symposium on Topics in Coding (ISTC)*, pages 1–5, 2023. DOI: [10.1109/ISTC57237.2023.10273526](https://doi.org/10.1109/ISTC57237.2023.10273526).

[50] Philip Andreasson, Joel Johansson, Simon Liljestrand, and Mats Granath. Quantum error correction for the toric code using deep reinforcement learning. *Quantum*, 3:183, 2019. DOI: [10.22331/q-2019-09-02-183](https://doi.org/10.22331/q-2019-09-02-183).